Articles

Urea-Driven Conformational Changes in Surface-Bound Superoxide Dismutase

Taewook Kang,[†,a] Surin Hong,[a] Inhee Choi, Jung-Joon Sung,[‡] and Jongheop Yi[*]

School of Chemical and Biological Engineering, Institute of Chemical Processes, Seoul National University,
Seoul 151-744, Korea. [*]E-mail: jyi@snu.ac.kr
[†]Department of Chemical and Biomolecular Engineering, Sogang University, Seoul 121-742, Korea
[‡]Department of Neurology, Seoul National University Hospital, Seoul 100-744, Korea

Both surface plasmon resonance (SPR) spectroscopy and atomic force microscopy (AFM) have been used to observe the change in Cu/Zn superoxide dismutase (SOD1) tethered to a Au film upon urea-induced denaturation. Exposure to a urea solution causes denaturation of SOD1, which shifts the minimum in the SPR curve to a larger angle without any change in reflectivity at the resonant angle (θ_{SPR}) for different urea concentrations. The differential reflectivity at θ_{SPR} ($\Delta(R_{min}/R_o)$) increases sigmoidally as a function of urea concentration becoming saturated at concentrations above 4 M. With the assumption of a two-state model for the denaturation of SOD1, the Gibbs free energy change for the denaturation of SOD1 on the Au surface is estimated to be ΔG^o = 1.8 ± 0.7 kcal/mol, which is lower by approximately one order of magnitude than that of SOD1 in the bulk solution. The immobilized SOD1 on the Au surface can be reversibly denatured and renatured. Consistent with calculations based on Fresnel equations for a multilayer system, liquid-AFM images show that upon denaturation, the thickness of the tethered SOD1 increases by *ca.* 2.0 times. Thus, SOD1 on the Au film tries to stretch its polypeptide chain in the vertical direction on unfolding.

Key Words : Atomic force microscopy (AFM), Conformational change, Superoxide dismutase (SOD1), Surface plasmon resonance (SPR), Urea

Introduction

There is growing interest in chip-based, high-throughput screening strategies for characterizing of the function and interactions of proteins owing to the compositional complexity and dynamic nature of the proteins of interest. The chip-based format allows for the massive, rapid, and parallel screening of thousands of biomolecular events in a single experiment.[1-5] Despite the growing success in such an *in vitro* immobilization of proteins, the prediction of how specific proteins will behave when tethered to a certain substrate remains a central challenge. In certain cases, conventional immobilization methods (such as physical adsorption or covalent binding through lysine and cysteine residues) render the active sites of proteins inaccessible or even denature proteins.[6] Moreover, immobilized proteins may not retain their function because of nonspecific interactions between the protein and the surface.[7,8] Therefore, a primary challenge in developing model surfaces *in vitro* is the development of methods that allow the structure and physiological function of surface-bound proteins to be estimated while permitting natural biological interactions to occur in such a manner that the results can be interpreted clearly and are related to biological events *in vivo*.

Conformational changes in proteins have been analyzed in great detail by circular dichroism (CD),[9-11] nuclear magnetic resonance (NMR),[13] small-angle X-ray scattering (SAXS),[14] and fluorescence energy transfer (FET).[15] However, most of the current methodologies were developed to measure the conformational behavior of proteins that are dispersed uniformly in solution and they are unsuitable for the detailed characterization of their counterparts in an interface, such as immobilized proteins. Nevertheless, the conformational dynamics (morphology) of proteins at the interface is important biologically (*e.g.*, integral membrane proteins) as well as in engineered systems for biosensors and biocatalysts, in which immobilized proteins are used. This is particularly true for proteins whose folding dynamics are closely linked to the pathogenesis of neurodegenerative diseases (*e.g.*, superoxide dismutase (SOD)[9] and α-synuclein[16]).

Cu/Zn superoxide dismutase (SOD1), a 32-kDa homodimeric protein, is expressed predominantly in the cytosol and decreases the intracellular concentration of superoxide radicals (O_2^-) by catalyzing their dismutation to O_2 and H_2O_2. Each subunit of the molecule binds one zinc atom and one copper atom. Interest in Cu/Zn SOD has been heightened by the finding that a major portion of familial amyotrophic lateral sclerosis (ALS-Lou Gehrig's disease) can be linked to mutations in the Cu/Zn SOD gene.[17] The discovery of a point mutation in the gene coding for Cu/Zn SOD1 in

subsets of familial cases provided much hope for the rapid development of therapies. Since then, most familial ALS (fALS) research has been directed toward elucidating the mechanism of this SOD1-mediated disease.[9,18-21] Because the fALS mutations are scattered throughout the primary sequence and three-dimensional structure of SOD1, there is considerable interest in the development of chip-based approaches for both basic biological research and commercial high-throughput screening of SOD1 in order to track the toxic gain-of-function of SOD1.

Here we report on the use of surface plasmon resonance (SPR) spectroscopy and atomic force microscopy (AFM) as a better cross check to quantitatively and qualitatively characterize urea-driven conformational changes in SOD1 immobilized on a Au surface. Surface plasmon resonance (SPR) is a phenomenon that occurs when linearly polarized light whose electric field vector is perpendicular to the surface (p-polarized) propagates from a medium having a high refractive index toward an interface with a material having a low refractive index.[22] The SPR-based characterization technique is based on the utilization of a noble metal to generate a surface plasmon electric field, which is then used to probe changes in the optical properties. *e.g.*, by a binding reaction, that occurs in the proximity of the surface.[23-29] The probe in SPR spectroscopy is a non-destructive interfacial electric field and is spatially distributed with an exponential decay from the metal surface (the characteristic decaying length of the field, δ_d, which is of the order of one-third the wavelength of the light involved). SPR responses (the position of surface plasmon resonance angle, θ_{SPR}, the width of the SPR plot, and the reflectivity $(R/R_o)_{min}$ at θ_{SPR}, for which R/R_o is a minimum) are highly sensitive to changes in the dielectric constant and the thickness of the material that is in contact with the metal surface. Because the protein folding/unfolding states would lead to a change in the local average refractive index of immobilized proteins,[8,30,31] it should be feasible to utilize SPR to monitor the urea-induced denaturation of SOD1 when it is tethered to a surface.

AFM has been widely used to visualize biological molecules, allowing morphological and mechanical information at the nanometer level. Particularly, the use of AFM to examine in biological or chemical samples in liquid media can be very useful, because (i) the oscillating energy activated between the tip and sample in the tapping mode are reduced, and (ii) structural changes in macromolecules can be observed in their native environment.

In the present study, thermodynamic stability of the surface-bound SOD1, defined as the decrease in the Gibbs free energy for denaturation from conformational transition curves induced by chemical denaturants at a constant pH and temperature was estimated using SPR measurements. In addition, we also performed atomic force microscopy (AFM) in a liquid environment to determine changes in the physical dimensions of SOD1 immobilized on the Au surface during the denaturation process.

Materials and Methods

Materials. 11-Mercaptoundecanoic acid (MUA. Sigma-Aldrich). *N*-(3-dimethylaminopropyl)-*N'*-ethylcarbodiimide hydrochloride (EDC, Aldrich), and *N*-Hydroxysuccinimide (NHS. Sigma-Aldrich) were used as received. Urea (Sigma), a denaturant, was dissolved in 25 mM potassium phosphate buffer (PBS. pH 7.4) to prepare urea solutions of different concentrations up to 5 M. H_2O was purified to above 18 MΩ using a Milli-Q water system (Millipore).

SPR instrumentation. Figure 1a shows a schematic diagram of the reaction cell used in the SPR instrumentation. A flow cell is mounted on the sensor/prism assembly so that solutions of sensing interest can be introduced easily to flow across the Au surface and that switching between different solutions can be accomplished rapidly. We utilized a five-phase, denoted as a (01234) SPR system in the Kretschmann configuration using attenuated total reflection (ATR). The different phases are labelled as follows: 0. BaK prism (n = 1.566706); 1. a layer of Au thin film (50 nm); 2. a carboxylic acid-terminated self-assembled monolayer (SAM) of MUA; 3. a layer of supported SOD1; 4, an ambient dielectric medium of buffer (25 mM PBS buffer). Time-resolved SPR angle shifts were measured using the fixed angle method which enabled the reflectance change ΔR to be linearly correlated with the SPR angle shift. $\Delta\theta_{SPR}$.[32] Reflectance data at a fixed incident angle were acquired in real time on a computer. For further calculations, the angle of incidence (θ in Figure 1a) was determined using Snell's law ($n_i \sin\theta_i = n_j \sin\theta_j$).

SOD1 purification. Human SOD genes encoding the wild type were cloned into the pET23b(+) (Novagen) vector and the proteins were expressed in *E. coli* BL21(DE3)-pLysS.[33] Cultures were induced by 0.5 mM isoprophyl b-D-thiogalactopyranoside for 3 to 6 h at 30 °C, and the cells were lysed by sonication in a buffer containing 150 mM NaCl, 50 mM Tris-HCl (pH 8.0), 0.1 mM EDTA, 1 mM dithiothreitol (DTT), and 1 mM phenylmethylsulfonyl fluoride (PMSF). Solid $(NH_4)_2SO_4$ was added to the cell extracts to ~50% saturation (0.313 g/mL). After centrifugation, the supernatant proteins were loaded on a phenyl-sepharose 6 Fast Flow high sub hydrophobic column (Amersham Biosciences). Proteins were eluted with a linear gradient of ammonium sulfate (0.75-0 M) in 50 mM sodium phosphate (pH 7.0). 150 mM NaCl, 0.1 mM EDTA and 0.25 mM DTT. Wild-type SOD1 was released with a high specificity from the column between 1.3 and 0.8 M ammonium sulfate. Demetalation and serial reconstruction of Zn and Cu metals were performed as described previously.[33]

Human SOD1 immobilization on the Au thin film. The immobilization procedures utilized carboxylate-modified (MUA-coated) surfaces to covalently attach proteins to the Au thin film *via* traditional carbodiimide coupling to protein-free amine moieties.[31,34,35] A typical protein immobilization procedure begins with formation of an active ester at the surface, produced by reacting 100 μL of a 100 mM, pH 5.5,
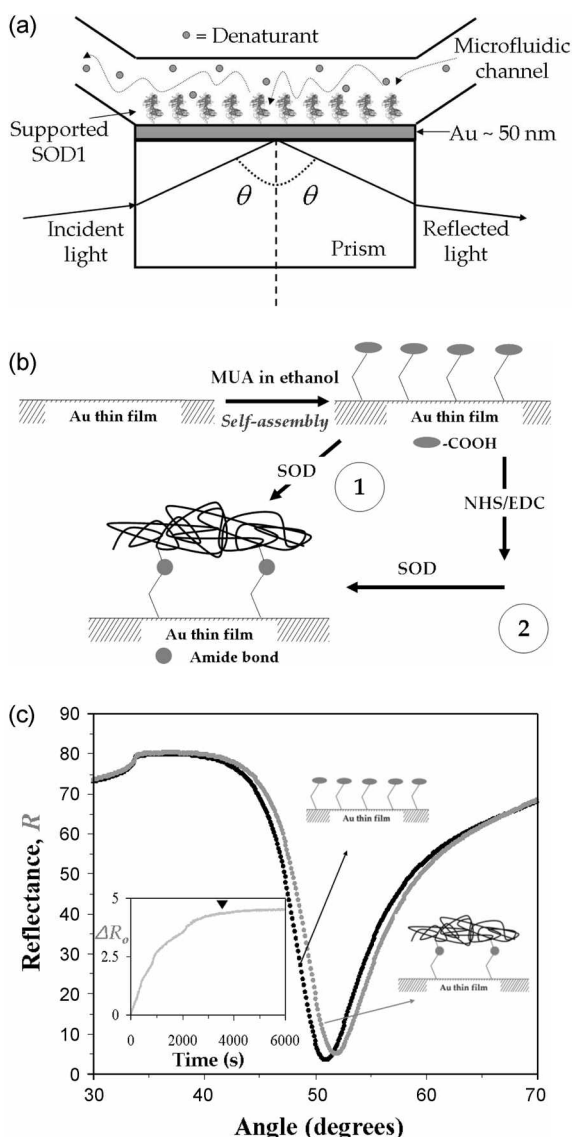
Figure 1. (a) Schematic diagram of a surface plasmon resonance setup. The incoming light is reflected to a detector by the Au thin film, which is evaporated on a BaK prism. (b) Schematic illustration of the binding reactions involved in the present study (pathway 2), including the self-assembly of MUA, the formation of an NHS ester, and SOD1 immobilization (not drawn to scale). It is well known, that in the MUA system, SOD1 immobilization is subjected to preactivation of the carboxyl groups with EDC/NHS reagents, the role of which is to activate the carboxyl groups to form O-acylurea intermediates and NHS esters that promote the formation of amide bonds with amino groups on the protein. Similar results (*e.g.*, SPR responses and AFM images) were obtained when using independent preparation (pathway 1). (c) The incident angle dependent SPR contour plots obtained from the MUA-Au surface, after the immobilization of SOD1, using an ambient dielectric of 25 mM PBS buffer. For each graph, every fourth point from the raw data collected is plotted to preserve the clarity of the contour plot. The inset cartoons represent the corresponding surface status. The inset figure represents the time-resolved SPR response for the immobilization of SOD1 on the Au surface.

EDC solution with the carboxylated surface for 15 min. The overall experimental procedures are summarized in Figure

1b (pathway 2). Briefly, a self-assembled monolayer (SAM) of MUA on the Au thin film was formed by treatment with a 1 mM MUA ethanolic solution for 18 h. The formation of an MUA monolayer was investigated by SPR measurements and Auger electron spectroscopy (AES). For the immobilization of SOD1 on the MUA treated Au thin film by covalent bonding, the MUA treated surface was first activated by a 7 min exposure to a 1:1 mixture of 0.4 M EDC and a 0.1 M aqueous solution of NHS. SOD1 (0.1 mM), in the same buffer solution, was then used for the immobilization (4 h). The immobilization of SOD1 was investigated by angle-resolved and time-resolved SPR measurements. At saturation, the surface was rinsed with copious amounts of water and buffer solution. It should be noted that the direct self-assembly of SOD1 to the Au surface (*i.e.*, covalent binding through cysteine residues of SOD1 (pathway 1 in Figure 1b)[36,37]) also gives identical SPR responses to those prepared by pathway 2 if the immersion time exceeds 12 h.

Liquid-AFM characterization. To scan a sample in the liquid phase, commercially applicable liquid cells have been developed by several researchers. In this work, an open liquid-cell system was used in conjunction with a commercial AFM instrument (XE-100, PSIA, Korea). To minimize intrinsic distortion of the apparatus, an independent *z*-scanner was used, which also eliminates the *x-z* cross coupling problem that is inherent in conventional AFM. Images of the wild-type SOD1 were analyzed in PBS buffer with an NSC36B (MikroMasch, Estonia).

Results and Discussion

SOD1 immobilization on the Au surface. Prior to investigating the denaturation effect of urea on SOD1, it was necessary to confirm that SOD1 was assembled on the surface of the Au thin film. The procedures were monitored during the attachment of SOD1 by both time- and angle-resolved SPR. Figure 1c shows time-resolved (inset curve) and angle-resolved SPR curves for the SOD1 prepared using an ambient dielectric of 25 mM PBS buffer. SOD1 began to be adsorbed immediately after the Au surface came into contact with the SOD1 solution (0.1 mM), forming a saturated film in about 1 h, which moved the angle-resolved SPR data by 0.5° to larger angles.

For a four-layered (approximated as a stacked Fresnel system) architecture as defined in Figure 1a (prism/Au/SOD1/dielectric medium), the angle change in the SPR response can be approximated as[38]

$$\Delta \theta_{SPR} \propto k_o \left(\frac{\varepsilon_{SOD1layer} - \varepsilon_{SOD1layer}}{\varepsilon_{SOD1layer}} \right) \left(\frac{\varepsilon_{SOD1layer} - \varepsilon_{Au}}{\varepsilon_{dielectric} - \varepsilon_{Au}^r} \right)$$

$$\times \left(\frac{2\pi d_{SOD1layer}}{\lambda} \right) \quad (1)$$

where k_o is the wave vector in the absence of SOD1 and ε_{Au}^r is the real part of the dielectric constant of Au, ε_{Au} (*i.e.*, $\varepsilon_{Au} = \varepsilon_{Au}^r + i\varepsilon_{Au}^i$). As can be seen in eq. (1) above, the SPR

resonance angle (θ_{SPR}) increases as a function of both the thickness ($d_{SOD1layer}$) and the dielectric constant ($\varepsilon_{SOD1layer}$) of the adlayer of SOD1 on the Au film. Therefore, the introduction of SOD1 with a higher dielectric constant of *ca.* 2.0 (typical dielectric constant of proteins) to the surface of the Au thin film than that of buffer are responsible for the increase in θ_{SPR} in Figure 1c. To ensure appropriate visual correlation with the SPR data for the immobilization of SOD1 to the Au surface, an SOD1-immobilized Au thin film was utilized as a substrate for the AFM measurements. Figure 2a shows an AFM topographic image (taken in air) of the bare Au thin film that had been thermally evaporated on the glass. When compared with the bare Au surface, the two distinct features after the immobilization of SOD1 are an increase in (1) nominal height in terms of the apparent increase in bright area (red arrow) and (2) an increase in the root-mean-square (rms) roughness. A minor corrugation in the surface of the film can be seen with the rms roughness in 1 μm $\times$ 1 μm areas of 0.6 nm. Modifying the Au substrate with SOD1 (Figure 2b) increases the surface roughness from 0.6 to 1.4 nm and gives images that appear devoid of aggregates.

Determination of the amount of the supported SOD1. Once the average thickness, d_{eff} (*surface*), of a uniform SOD1 layer is assumed to be the diameter of SOD1 (Although dimeric SOD1 is a rather elongated ellipsoid about 33 Å wide, 67 Å long, and 36 Å deep,[36,39] the morphology of SOD1 was assumed to be equivalent to a spherical inclusion with a radius of 21.5 Å as in Figure 3 bottom), in order to correlate the SPR angle change ($\Delta\theta_{SPR}$) to the amount of the immobilized SOD1 on the Au surface, the Maxwell and Garnett theory was employed here on the basis of neglecting the possible anisotropy of the supported SOD1 layer.[40]

$$\frac{(\varepsilon_{eff} - \varepsilon_{buffer})}{(\varepsilon_{eff} + 2\varepsilon_{buffer})} = \beta f \text{ where } \beta = \frac{(\varepsilon_{SOD1} - \varepsilon_{buffer})}{(\varepsilon_{SOD1} + 2\varepsilon_{buffer})} \quad (2)$$

Here f is the volume fill fraction occupied by the inclusion of SOD1 and ε_{buffer} and ε_{SOD1} are the dielectric constants of PBS buffer and SOD1 in the native state, respectively.

For the multilayer model employed here, n represents the layer number, which is given the value of 0, 1, 2, 3, 4 for the prism, Au layer, MUA SAM, SOD1 layer, and the dielectrics (either 25 mM PBS buffer or SOD1 + PBS buffer). The optical properties of the layers 1 (Au) and 2 (MUA) were obtained from the literature.[26,41] Using these parameters as an initial starting condition, d_1, d_2, ε_1, and ε_2 were calculated by optimizing the simulated line for fitting to the experimental data in an iterative manner. For a [014(SOD1 + PBS buffer)] system, the simulated fit (calculation based on applying Fresnel equations to a multilayered system) to the measured values of the surface plasmon angle (the SPR responses were measured in both the SOD1 solution and PBS buffer in contact with the bare Au surface), θ_{SPR} and the observed shift in the SPR contour plots with an iteration method in Winspall II (Fresnel equation solver, MPIP, Germany) give that ε_{eff}^{bulk} = 1.854 for case 1 in Figure 3.[42] For the [01234(PBS buffer)] system, we find, by similar
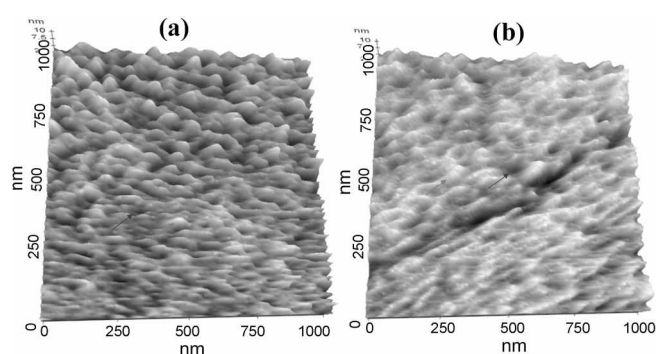
Figure 2. Representative AFM topographic images (image size: 1 μm $\times$ 1 μm) taken in air for (a) a native Au substrate and for (b) the Au substrate after the immobilization of SOD1. Red and blue arrows in (a) exhibit surface roughness. On the other hand, after the immobilization of SOD1, the overall increase in bright area (red arrow in (b) becomes apparent.
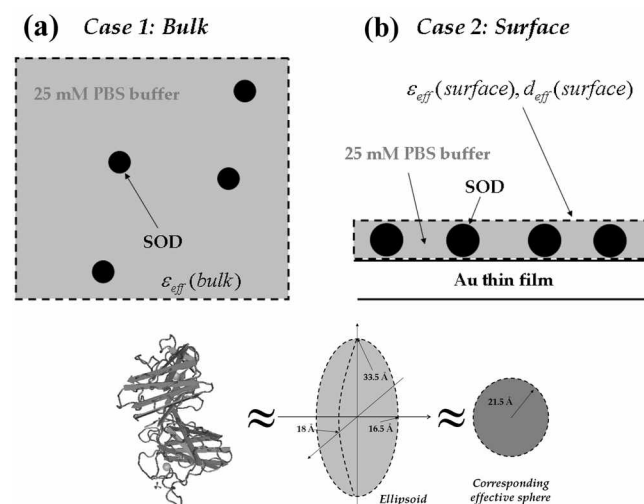
Figure 3. (a) Schematic diagram of Maxwell Garnett composite geometry consisting of SOD1 randomly dispersed in a host material (PBS buffer of 25 mM) (b) Schematic diagram of an interface involving the 2-D confined SOD1 of thickness d_{eff} (*surface*) and dielectric constants ε_{eff}(*surface*) directly on the Au probe surface.

measurements, that $\varepsilon_{eff}^{surface}$ = 2.029 for case 2 in Figure 3.

Once we determined ε_{eff}^{bulk}, $\varepsilon_{eff}^{surface}$ for each case, we used simple algebra to determine the relative amount of SOD1 adsorbed to the surface. Using the Maxwell-Garnett equation, it is possible to relate the measured dielectric constants ε_{eff}^{bulk}, $\varepsilon_{eff}^{surface}$ to N, the relative number of SOD per unit area, which links to the volume fraction of SOD1 on the Au surface, $f_{surface}$

$$f_{surface} = \frac{(\varepsilon_{eff}^{surface} - \varepsilon_{buffer})}{(\varepsilon_{eff}^{surface} + 2\varepsilon_{buffer})} \frac{(\varepsilon_{SOD} - \varepsilon_{buffer})}{(\varepsilon_{SOD} + 2\varepsilon_{buffer})} \quad (3)$$

On the other hand, the volume fraction of SOD1 in the bulk solution would simply be

$$f_{bulk} = \frac{(\varepsilon_{eff}^{surface} - \varepsilon_{buffer})}{(\varepsilon_{eff}^{surface} + 2\varepsilon_{buffer})} \frac{(\varepsilon_{SOD} - \varepsilon_{buffer})}{(\varepsilon_{SOD} + 2\varepsilon_{buffer})} \quad (4)$$
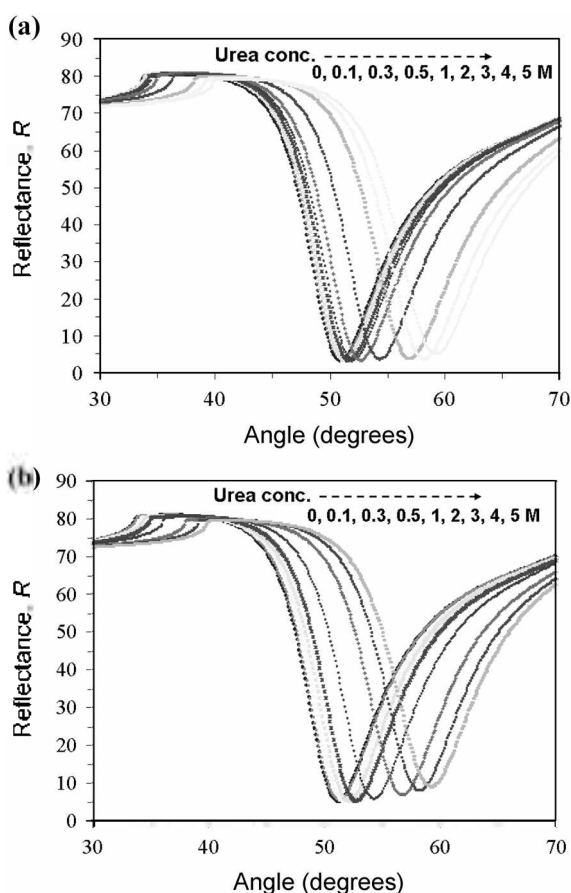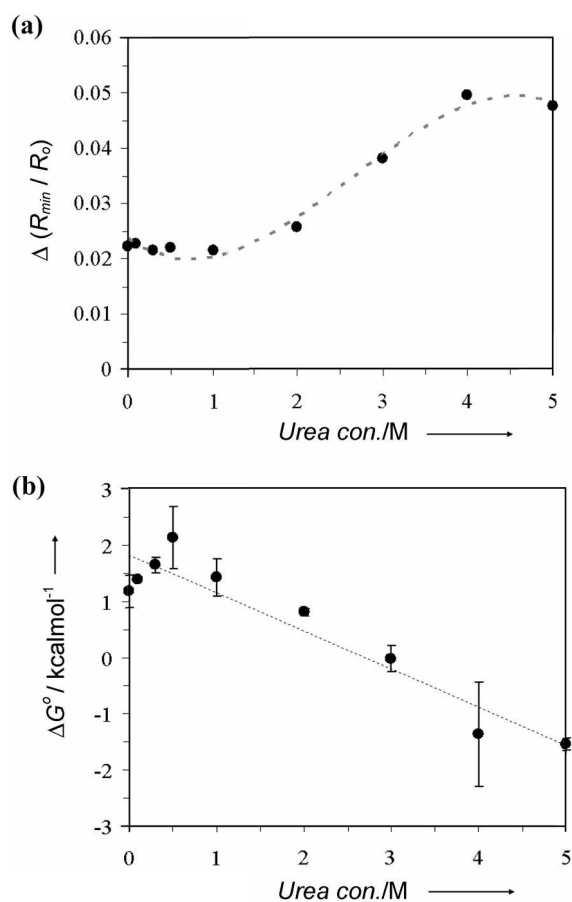
Figure 4. (a) Angle-resolved SPR curves as a function of urea concentration (a) for SOD1/Au and (b) for bare Au. Both curves shift to right at high concentrations of urea. Reflectivity at resonance angles for the bare Au moves upward whereas that for the SOD1/Au shows no change.

Figure 5. (a) $\Delta(R_{min}/R_o)$ versus urea concentration from 0 to 5 M. (b) Gibbs free energy change ΔG^o versus urea concentration, derived from the experimental data in (a). The value of ΔG^o for the denaturation of the tethered SOD1 on the Au was calculated to be 1.8 ± 0.7 kcal/mol.

Thus, when eq. (3) is divided by eq. (4), the SOD excess surface concentration is $f_{surface}/f_{bulk} = 30$. The volume fraction of SOD1 is about 25% of the estimated close-packed coverage. This value converts to a SOD1 concentration on the surface of 0.82×10^{-7} g/cm^2. On the basis of an evenly distributed SOD1 arrangement with periodic square lattices, the center-to-center interparticle spacing between neighboring SOD1 particles is estimated to be 8 nm, which suggests that the supported SOD1 molecules in the native state do not overlap with each other.

SPR contour plots for urea-induced denaturation. The SPR plots (Figure 4a) for the urea-triggered denaturation of SOD1 tethered to the Au (SOD1/Au) proportionally shift to the right depending on the urea concentration without any change in reflectivity at the resonant angles. On the contrary, SPR curves measured for the bare Au (control experiment, data are also presented for the bare Au, which was not denatured by urea) showed not only a shift to the right but also a measurable increase in reflectivity at the resonant angle up to a concentration of 5 M urea, followed by no further changes above 5 M urea.[43]

It should be noted that the SPR responses (The position of θ_{SPR}, and the reflectivity (R_{min}/R_o) at θ_{SPR}) in both SPR

curves arise from the contributions of both the change in the bulk dielectric constant of the urea concentration which is evident from the sequential shift in the critical angle to the right and the conformational change in SOD1 that is induced by urea. In order to differentiate between these two contributions, the SPR responses at each urea concentration for bare Au were subtracted from the SPR responses for SOD1/Au to form the difference, providing two sets of plots of both the differential reflectivity at θ_{SPR} $(\Delta(R_{min}/R_o))$ $[\Delta(R_{min}/R_o)_{urea=x} = (R_{min}/R_o)_{bare\ Au,\ urea=x} - (R_{min}/R_o)_{SOD1,\ urea=x}$, where x (M) is in the range of 0-5] and the differential SPR angle change $(\Delta\theta_{SPR})_{net}$ $[(\Delta\theta_{SPR})_{net,urea=x} = (\Delta\theta_{SPR})_{bare,urea=x} - (\Delta\theta_{SPR})_{SOD1:Au,urea=x}]$ versus urea concentration.

The experimental data shown in Figure 5a show a sigmoidal increase in $\Delta(R_{min}/R_o)$ with increasing concentration of urea. $\Delta(R_{min}/R_o)$ gradually increases as a function of urea concentration and becomes saturated above 4 M, whereas $(\Delta\theta_{SPR})_{net}$ is not dependent on the presence of urea in the concentration range 0-5 M (data not shown). The commonly seen shifts to the right are caused by the urea solutions. However, the upward shifts of $\Delta(R_{min}/R_o)$ cannot be explained by the change in the dielectric constant of the solution itself. Therefore, we conclude that the observed

shifts in $\Delta(R_{min}/R_o)$ mirror the urea-induced conformational changes of SOD1.

In order to estimate the value of ΔG^o of the immobilized SOD1 from denaturation curves, we assumed a two-state model in the derivation of eq. (5). The reflectivity data in Figure 5a were fitted using the following linear combination.

$$\Delta \frac{R_{min}}{R_o} = (f_N)\left(\Delta \frac{R_{min}}{R_o}\right)_N + (f_D)\left(\Delta \frac{R_{min}}{R_o}\right)_D \qquad (5)$$

where $\Delta(R_{min}/R_o)_X$ is the change in reflectivity and f_X is the fraction of SOD1 in state X where N represents the native state and D corresponds to the denatured state (*i.e.*, $f_D + f_N = 1$). The values for these variables were determined from data for each concentration of urea. From the data presented in Figure 5a, subject to the assumption of a two-state model of SOD1 denaturation, the optical data in Figure 5a were converted into the Gibbs free energy change (ΔG^o) for the denaturation of the surface-confined SOD1 using the relation.

$$\Delta G^o = -RT \ln K_{equilibrium} = -RT \ln \frac{f_D}{f_N} = -RT \ln \frac{f_D}{1 - f_D} \qquad (6)$$

Figure 5b shows a plot of ΔG^o as a function of urea concentration. From the linear extrapolation, an offset of ΔG^o for the surface-confined SOD1 was calculated to be 1.8 $\pm$ 0.7 kcal/mol.[9, 44]

Denaturation/renaturation reversibility. Most proteins seldom recover their activity after they are denatured, especially at a solid surface, but the ability to renature is an important factor when they are considered as catalysts or sensors. The SPR response for the urea-induced denaturation of surface-bound SOD1 (see supporting information) shows an increase in maximum reflectance as a function of urea concentration in the range of 0.1-2 M. The sequential renaturation of the supported SOD1 by dilution of the urea restored its initial SPR spectra, suggesting that the urea-induced changes at the Au surface are essentially reversible.

Elongation of the supported SOD1 dimension. Figure 6 shows liquid-AFM images of the Au surface (same area) after modification with SOD1 (Figure 6a) and after allowing for denaturation by urea to take place with SOD1 for 30 min at 25 °C (Figure 6b). It should be noted that the two images were taken at the same location. Upon denaturation, there is barely any change in morphology. Nevertheless, the vertical height increases significantly, to about 4 nm (the apparent increase in height profile). The cursor plot of Figure 6c exhibits this typical increase in the nominal height of the tethered SOD1 upon the incubation with urea. This behavior suggests that upon urea-driven denaturation a SOD1 molecule has stretched its polypeptide chain vertically, but not horizontally. It has been reported that upon heat-driven denaturation, the radius of gyration (R_g) of SOD in the bulk is increased by threefold over its value in the native state.[45] Considering the restricted conformational plasticity of the surface-confined SOD1 as the result of the possibility of tilted orientation, multiple binding (amide bond formation) to the Au surface, and AFM tip compression, this twofold increase is in satisfactory agreement with the literature.
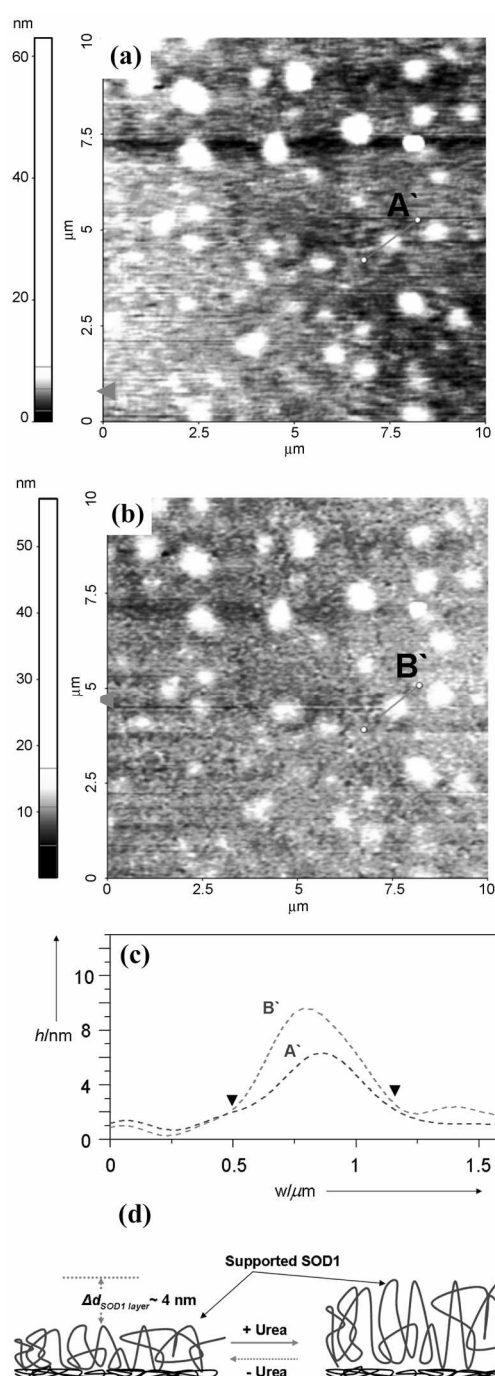
Figure 6. Liquid-atomic force microscopy images (same area) of SOD1/Au prior to exposure to the urea solution (b) for SOD1/Au after treatment with 4 M urea. The two images were taken at the same location. The apparent increase in height profiles is highlighted by red triangle. (c) represents corresponding typical linear scans along the scan direction indicated in (a) and (b). (d) Schematic representation of the change in the morphology of tethered SOD1 upon urea treatment.

The simulated fit (calculation based on applying Fresnel equations to a homogeneous and multilayered system) to the measured values of θ_{SPR} and the observed shift of SPR contour plots in Figure 4a reveals that the thickness of a fully denaturated SOD1 corresponds to approximately 10 nm at a 4 M concentration of urea, and collapses to a 4.3 nm thick
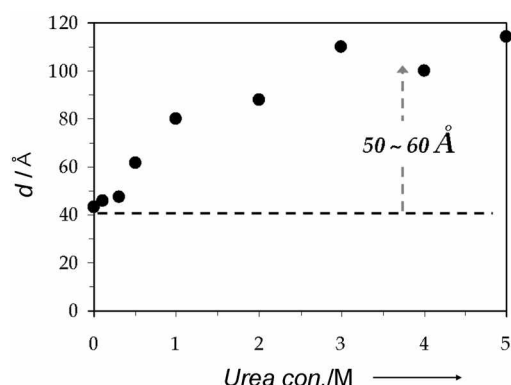
Figure 7. Calculated adlayer (the immobilized SOD1) thickness d, for the interface structure of Figure 3b, for the special case where $\varepsilon_{eff}(surface)$ = constant upon the denaturation. Calculation with Maxwell's equations and thin-film optical model to achieve the best fit to the experimental SPR curves.

film when the urea is absent (Figure 7).[46] This result also suggests that the average distance between any two amino acid residues (i.e., R_g) of the tethered SOD1 in the denatured state is approximately 2-3 times more that in the native state, which is consistent with the liquid-AFM analyses.

Conclusions

On the basis of SPR and AFM results, we have demonstrated that (1) calculation of the effective dielectric constants from the measured SPR response to a layer of adsorbed SOD1 on the Au determines the fractional SOD1 coverage on the surface, (2) the urea-driven denaturation and renaturation of the supported SOD1 at the Au interface are quite reversible, as evidenced by monitoring the *in situ* SPR curves, (3) the differential SPR reflectivity $\Delta(R_{min}/R_o)$ allows us to estimate the value of ΔG^o for the denaturation of the supported SOD1, and (4) the thickness of the supported SOD1 markedly increases with exposure to a urea solution. The population density of SOD1 on the Au is calculated to be 82 ng/cm². ΔG^o for the denaturation of the surface-bound SOD1 is 1.8 ± 0.7 kcal/mol, about 10 times less than that in the free state. The twofold increase in the thickness of the surface-confined SOD1 caused by the denaturation found from analyzing liquid-AFM images is in good agreement with the calculated results. This unidirectional movement of the immobilized SOD1 in response to the stimulus may have useful applications, such as solid-state sensors and bionanomechanical devices. From a biological point of view, these characterization techniques of surface-confined SOD1 leads to a common first step in understanding the physiological function of SOD1 in the pathology of SOD1 mutations and ALS via the *in vitro* immobilization. On the other hand, our approach may find a potential to develop SOD1-based engineered systems; however, it need not be restricted to SOD1. The findings herein suggest that these techniques can be extended for the usage of the characterization of many other supported biomolecules.

Supporting Information Available. "*In-situ* (time-resolved) SPR measurements of urea-driven denaturation and renaturation for SOD1/Au as a function of urea concentration." are available on request from the correspondence author.

References

1. Phizicky, E.; Bastiaens, P. I.; Zhu, H.; Snyder, M.; Fields, S. *Nature* **2003**, *422*, 208.
2. Zhang, K.; Diehl, M. R.; Tirrell, D. A. *J. Am. Chem. Soc.* **2005**, *27*, 10136.
3. MacBeath, G.; Schreiber, S. L. *Science* **2000**, *289*, 1760.
4. Haab, B. B.; Dunham, M. J.; Brown, P. O. *Genome Biol.* **2001**, *2*, 1.
5. Nielsen, U. B.; Cardone, M. H.; Sinskey, A. J.; MacBeath, G.; Sorger, P. K. *Proc. Natl. Acad. Sci. USA* **2003**, *100*, 9330.
6. Zhu, H.; Snyder, M. *Curr. Opin. Chem. Biol.* **2003**, *7*, 55.
7. Sadana, A. *Chem. Rev.* **1992**, *92*, 1799.
8. Chah, S.; Kumar, C. V.; Hammond, M. R.; Zare, R. N. *Anal. Chem.* **2004**, *76*, 2112.
9. Lindberg, M. J.; Normark, J.; Holmgren, A.; Oliveberg, M. *Proc. Natl. Acad. Sci. USA* **2004**, *101*, 15893.
10. Baskakov, I. V.; Legname, G.; Prusiner, S. B.; Cohen, F. E. *J. Biol. Chem.* **2001**, *276*, 19687.
11. Gupta, R.; Ahmad, F. *Biochemistry* **1999**, *38*, 2471.
12. Harper, S. M.; Neil, L. C.; Gardner, K. H. *Science* **2003**, *301*, 1541.
13. Eliezer, D.; Jennings, P. A.; Wright, P. E.; Doniach, S.; Hodgson, K. O.; Tsuruta, H. *Science* **1995**, *270*, 487.
14. Ohba, S.; Hosomi, H.; Ito, Y. *J. Am. Chem. Soc.* **2001**, *123*, 6349.
15. Rischel, C.; Poulsen, F. M. *FEBS Lett.* **1995**, *374*, 105.
16. Cole, N. B.; Murphy, D. D.; Grider, T.; Rueter, S.; Brasaemle, D.; Nussbaum, R. L. *J. Biol. Chem.* **2002**, *277*, 6344.
17. Rosen, D. R.; Siddique, T.; Patterson, D.; Figlewicz, D. A.; Sapp, P.; Hentati, A.; Donaldson, D.; Goto, J. *Nature* **1993**, *362*, 59.
18. Julien, J. P. *Cell* **2001**, *104*, 581.
19. Rakhit, R.; Crow, J. P.; Lepock, J. R.; Kondejewski, L. H.; Cashman, N. R.; Chakrabartty, A. *J. Biol. Chem.* **2004**, *279*, 15499.
20. Stathopulos, P. B.; Rumfeldt, J. A. O.; Scholz, G. A.; Irani, R. A.; Frey, H. E.; Hallewell, R. A.; Lepock, J. R.; Meiering, E. M. *Proc. Natl. Acad. Sci. USA* **2003**, *100*, 7021.
21. Aliyev, E.; Sakallioğlu, U.; Eren, Z.; Açıkgöz, G. *Biomaterials* **2004**, *25*, 4633.
22. Knoll, W. *Annu. Rev. Phys. Chem.* **1998**, *49*, 569.
23. Roy, D.; Fendler, J. H. *Adv. Mater.* **2004**, *16*, 479.
24. Chah, S.; Fendler, J. H.; Yi, J. *Chem. Commun.* **2002**, 2094.
25. Kang, T.; Moon, J.; Oh, S.; Hong, S.; Chah, S.; Yi, J. *Chem. Commun.* **2005**, 2360.
26. Chah, S.; Yi, J.; Pettit, C. M.; Roy, D.; Fendler, J. H. *Langmuir* **2002**, *18*, 314.
27. Kang, T.; Hong, S.; Moon, J.; Oh, S.; Yi, J. *Chem. Commun.* **2005**, 3721.
28. Wischerhoff, E.; Zacher, T.; Laschewsky, A.; Rekai, E. D. *Angew. Chem. Int. Ed.* **2003**, *39*, 4602.

29. Ekgasit, S.; Thammacharoen, C.; Knoll, W. *Anal. Chem.* **2004**, *76*, 561.

30. Sota, H.; Hasegawa, Y. *Anal. Chem.* **1998**, *70*, 2019.

31. Kang, T.; Hong, S.; Kim, H. J.; Moon, J.; Oh, S.; Paik, S. R.; Yi, J. *Langmuir* **2006**, *22*, 13.

32. Zacher, T.; Wischerhoff, E. *Langmuir* **2002**, *18*, 1748.

33. Boissinot, M.; Karnas, S.; Lepock, J. R.; Cabelli, D. E.; Tainer, J. A.; Getzoff, E. D.; Hallewell, R. A. *EMBO J.* **1997**, *16*, 2171.

34. Su, X.; Wu, Y. J.; Robelek, R.; Knoll, W. *Langmuir* **2005**, *21*, 348.

35. Lahiri, J.; Isaacs, L.; Tien, J.; Whitesides, G. M. *Anal. Chem.* **1999**, *71*, 777.

36. Tian, Y.; Mao, L.; Okajima, T.; Ohsaka, T. *Anal. Chem.* **2004**, *76*, 4162.

37. Tian, Y.; Mao, L.; Okajima, T.; Ohsaka, T. *Anal. Chem.* **2002**, *74*, 2428.

38. Sarkar, D.; Somasundara, P. *Langmuir* **2004**, *20*, 4657.

39. Tainer, J. A.; Getzoff, E. D.; Beem, K. M.; Richardson, D. C. *J. Mol. Biol.* **1982**, *160*, 181.

40. Gehr, R. J.; Boyd, R. W. *Chem. Mater.* **1996**, *8*, 1807.

41. Chah, S.; Hammond, M. R.; Zare, R. N. *Chem. Biol.* **2005**, *12*, 323.

42. This system represents the SOD1 in PBS over the bare Au surface. This was used to calculate the effective refractive index of the bulk solution (*i.e.*, SOD1 solution) based on the assumption of no interaction between SOD1 protein and the gold surface. However, during the immersion time course, it is likely that the protein will irreversibly adsorb onto and cover the Au surface to some extent. If this is the case, the value of the effective refractive index of the bulk solution obtained from the SPR spectrum will be far off caused by the additional contribution of the adsorbed SOD1 to the SPR spectrum. In order to minimize (or exclude) the possibility of the adsorption of SOD1 to this bare Au surface, we measured SPR spectrum within two minutes after the Au surface came into contact with SOD1 solution.

43. A non-specific reaction was checked by replacing bare Au thin film by MUA/Au thin film. No detectable interaction of the MUA/Au thin film with urea was found.

44. Lynch, S. M.; Boswell, S. A.; Colón, W. *Biochemistry* **2004**, *43*, 16525.

45. Khare, S. D.; Ding, F.; Dokholyan, N. V. *J. Mol. Biol.* **2003**, *334*, 515.

46. Upon the urea-induced denaturation, the dielectric constant of the supported SOD1 was assumed to be constant at a value of 2.03.